Use of a Chemical Trigger for Electron Transfer to Characterize a Precursor to Cluster **X** in Assembly of the Iron-Radical Cofactor of *Escherichia coli* Ribonucleotide Reductase†

Lana Saleh,‡ Carsten Krebs,§,⊥ Brenda A. Ley,‡ Sunail Naik,§ Boi Hanh Huynh,§ and J. Martin Bollinger, Jr.*,‡

Department of Biochemistry and Molecular Biology, The Pennsylvania State University, University Park, Pennsylvania 16802, and Department of Physics, Emory University, Atlanta, Georgia 30322

Received November 21, 2003; Revised Manuscript Received February 27, 2004

ABSTRACT: A key step in generation of the catalytically essential tyrosyl radical (Y122•) in protein R2 of *Escherichia coli* ribonucleotide reductase is electron transfer (ET) from the near-surface residue, tryptophan 48 (W48), to a $(Fe_2O_2)^{4+}$ complex formed by addition of O_2 to the carboxylate-bridged diiron(II) cluster. Because this step is rapid, the $(Fe_2O_2)^{4+}$ complex does not accumulate and, therefore, has not been characterized. The product of the ET step is a "diradical" intermediate state containing the well-characterized Fe(IV)Fe(III) cluster, **X**, and a W48 cation radical ($W48^{+•}$). The latter may be reduced from solution to complete the two-step transfer of an electron to the buried diiron site. In this study, a $(Fe_2O_2)^{4+}$ state that is probably the precursor to the **X**−$W48^{+•}$ diradical state in the reaction of the wild-type protein (R2-wt) has been characterized by exploitation of the observation that in R2 variants with W48 replaced with alanine (A), the otherwise disabled ET step can be mediated by indole compounds. Mixing of the Fe(II) complex of R2-W48A/Y122F with O_2 results in accumulation of an intermediate state that rapidly converts to **X** upon mixing with 3-methylindole (3-MI). The state comprises at least two species, of which each exhibits an apparent Mössbauer quadrupole doublet with parameters characteristic of high-spin Fe(III) ions. The isomer shifts of these complexes and absence of magnetic hyperfine coupling in their Mössbauer spectra suggest that both are antiferromagnetically coupled diiron(III) clusters. The fact that both rapidly convert to **X** upon treatment with a molecule (3-MI) shown in the preceding paper to mediate ET in W48A R2 variants indicates that they are more oxidized than **X** by one electron, which suggests that they have a bound peroxide equivalent. Their failure to exhibit either the long-wavelength absorption (at 650−750 nm) or Mössbauer doublet with high isomer shift (>0.6 mm/s) that are characteristic of the putatively μ-1,2-peroxo-bridged diiron(III) intermediates that have been detected in the reactions of methane monooxygenase (**P** or $\mathbf{H_{peroxo}}$) and variants of R2 with the D84E ligand substitution suggests that they have geometries and electronic structures different from those of the previously characterized complexes. Supporting this deduction, the peroxodiiron(III) complex that accumulates in R2-W48A/D84E is much less reactive toward 3-MI-mediated reduction than the $(Fe_2O_2)^{4+}$ state in R2-W48A/Y122F. It is postulated that the new $(Fe_2O_2)^{4+}$ state is either an early adduct in an orthogonal pathway for oxygen activation or, more likely, the successor to a (μ-1,2-peroxo)diiron(III) complex that is extremely fleeting in R2 proteins with the wild-type ligand set but longer lived in D84E-containing variants.

The R2 subunit of *Escherichia coli* ribonucleotide reductase (hereafter, simply R2[1]) is a member of the diiron-carboxylate family of oxidases and oxygenases (*1*−*3*). Proteins in this family have similar structures and carboxylate-bridged diiron(II) cofactors, which they employ to reductively activate molecular oxygen for difficult oxidation reactions. The two most extensively studied family members are R2 and soluble methane monooxygenase (sMMO). The former activates O_2 for introduction of its catalytically essential tyrosyl radical (Y122•) by one-electron oxidation of Y122 (*4*−*6*), whereas the latter hydroxylates methane (*7*−*10*). Detailed insights into the mechanisms of these two reactions have been obtained by direct detection and characterization of intermediate states. In the sMMO reaction, peroxodiiron(III) and diiron(IV) intermediates (**P** and **Q**, respectively) have been detected (*11*−*18*). **P** is thought to be a (μ-1,2-peroxo)diiron(III) complex (*13*, *14*, *16*) and **Q** a bis-(μ-oxo)diiron(IV) complex (*15*). Kinetic evidence indicates that they form in sequence and that **Q** hydroxylates methane (*11*, *12*, *14*−*18*). In the R2 reaction, only the

† This work was supported by grants from the Public Health Services (Grant GM55365 to J.M.B. and Grant GM47295 to B.H.H.).

* To whom correspondence should be addressed. Tel: (814) 863-5707. Fax: (814) 863-7024. E-mail: jmb21@psu.edu.

‡ Penn State University.

§ Emory University.

⊥ Present address: Department of Biochemistry and Molecular Biology, The Pennsylvania State University, University Park, PA 16802.

[1] Abbreviations: R2, R2 subunit of *Escherichia coli* ribonucleotide reductase; sMMO, soluble methane monooxygenase; MMOH, the hydroxylase component of sMMO; Y122•, tyrosine 122 radical; ET, electron transfer; wt, wildtype; $W48^{+•}$, tryptophan 48 cation radical; v/v, volume/volume; buffer A, 100 mM Hepes buffer, 10% (v/v) glycerol, pH 7.6; RFQ-EPR, rapid freeze-quench EPR; RFQ-Möss, rapid freeze-quench Mössbauer; 3-MI, 3-methylindole.

10.1021/bi036099e CCC: $27.50
Published on Web 05/01/2004

Fe(IV)Fe(III) cluster, **X**, has been definitively detected (*19*−*27*). It forms when the near-surface residue, W48, reduces an uncharacterized adduct (hereafter denoted $(Fe_2O_2)^{4+}$) between O_2 and the diiron(II) cluster (*21, 28*). Reduction of the W48 cation radical ($W48^{+\bullet}$) constituent of the resulting **X**−$W48^{+\bullet}$ "diradical" state by a variety of reductants (ascorbate, thiols, $Fe(II)_{aq}$) is facile (*28*), leaving cluster **X** to generate $Y122^{\bullet}$ in the final and slowest step of the reaction (*20, 29*).

Electron transfer (ET) from W48 is sufficiently rapid to have prevented accumulation and detection of the $(Fe_2O_2)^{4+}$ oxidant (*28*). Consequently, it has not been possible to establish with certainty whether the R2 and sMMO reactions proceed through one or more common intermediates or completely orthogonal pathways. Nevertheless, mounting indirect evidence has suggested that a common initial pathway is more likely. This evidence includes (1) the observations of a **P**-like peroxodiiron(III) complex and competing self-hydroxylation and Y122-oxidation reactivities in variants of R2 (*30*−*36*), (2) the detection of common, very short (∼2.5 Å) Fe−Fe distances in **Q** and **X** (*15, 27*), (3) the demonstration of γ-radiolytic cryoreduction of freeze-trapped **Q** to an Fe(IV)Fe(III) complex with marked spectroscopic similarity to cluster **X** (*37*), and (4) the assessment by computational methods that similar peroxodiiron(III) intermediates could form (*38*−*40*). Perhaps most compellingly, a long-wavelength (∼700 nm) optical absorption feature and one line of what could be a Mössbauer quadrupole doublet at a position consistent with an isomer shift of 0.66 mm/s were detected shortly (milliseconds) after initiation of the R2 reaction (*22*). These features are similar to those characterizing **P** (*13, 14, 16*) and the peroxodiiron(III) complex that accumulates in R2 variants with the D84E ligand substitution (*30*−*32, 41*). However, the modest accumulation of the putative peroxodiiron(III) complex made it difficult to establish its competence to be the precursor to the **X**−$W48^{+\bullet}$ state, and a later kinetic study called into question whether the detected species could be on the reaction pathway (*22, 28*). Moreover, even under the presumption that a **P**-like complex is part of the R2 reaction sequence, the point of divergence from the sMMO mechanism would not be obvious. No evidence has been obtained for a **Q**-like species in the R2 reaction, leaving open the alternative possibilities that the presumptive **P**-like complex in R2 might either undergo reduction itself by W48 to form **X** or isomerize to a distinct peroxodiiron(III) complex prior to the ET step.

Resolution of these issues by detection of the precursor to the **X**−$W48^{+\bullet}$ state in the R2 reaction has been a primary objective of our studies. Initially, O_2 activation was examined in W48-substituted R2 variants in the expectation that the "kinetically masked" intermediate would accumulate in the absence of the electron-shuttling residue (*42*). Indirect, kinetic evidence for the accumulation of a $(Fe_2O_2)^{4+}$ species was found. It oxidizes Y122 (instead of W48) to form a **X**−$Y122^{\bullet}$ diradical intermediate. The oxidation of Y122 by this species is 10-fold faster than that by **X** in the R2-wt reaction (*42*), underscoring the high intrinsic reactivity of the uncharacterized $(Fe_2O_2)^{4+}$ complex toward one-electron reduction. To confer even greater stability to this species and thereby facilitate its characterization, the R2-W48F/Y122F variant was prepared. Freeze-quench Mössbauer (RFQ-Möss) experiments on the reaction of this double variant revealed the rapid development and relatively slow decay of spectral features not associated with either reactant or product(s), but unfortunately, the multiplicity of these features (a reflection of the presence of multiple species) and their poor resolution from those associated with downstream products prevented unequivocal association of specific features with the reactive $(Fe_2O_2)^{4+}$ intermediate.[2] Moreover, even if such association had been achieved, proof of the chemical competence of this complex to be on the normal reaction pathway (i.e., to generate **X** upon its reduction) would not have been possible because electron transfer to the presumptive $(Fe_2O_2)^{4+}$ complex is so slow in this protein that very little **X** accumulates, making it difficult to demonstrate a precursor−product relationship.[2]

Scheme 1: Mechanism of O_2 Activation in R2−W48A/Y122F in the Presence of 3-MI ET Mediator

The development described in the preceding paper (*43*) of a method to reactivate ET by addition of a small molecule (3-methylindole or 3-MI) suggested an approach to surmounting each of these technical obstacles. We envisaged that exposure of the $(Fe_2O_2)^{4+}$ complex, preformed by mixing the Fe(II)−R2-W48A/Y122F complex with O_2, to the ET mediator might trigger conversion to **X** (Scheme 1). This chemical triggering would simultaneously permit kinetic resolution of the features of the intermediate complex(es) specifically reactive toward 3-MI-mediated one-electron reduction and demonstrate its (their) chemical competence to be on the pathway to **X**. In this article, we demonstrate the realization of this strategy and document that the spectroscopic signatures of the $(Fe_2O_2)^{4+}$ state that is triggered to convert to cluster **X** are distinct from those of known peroxodiiron(III) complexes (such as **P**) and the diiron(IV) intermediate, **Q**, in the sMMO reaction. While cognizant that 3-MI may not be triggering ET according to the intended mechanism (i.e., binding in the pocket created by truncation of the indole side chain of W48) and that the W48A and Y122F substitutions potentially could alter the O_2 activation pathway, we nevertheless propose that the detected state is identical to the kinetically masked precursor to the **X**−$W48^{+\bullet}$ state in the reaction of R2-wt. We suggest that it represents either an early adduct in a pathway for O_2 activation distinct from that beginning with the (μ-1,2-peroxo)diiron(III) complex or, more probably, a successor to the canonical peroxide complex.

MATERIALS AND METHODS

Materials. Materials were obtained from the sources listed in the preceding manuscript (*43*).

Preparation and Quantitation of Apo R2−*W48A/Y122F.* pR2-W48A/Y122F, the overexpression vector for R2-W48A/Y122F, was prepared from pR2-Y122F (*20, 29*), pR2-W48F (*42*), and pR2-W48A (*43*). The 358 base pair *Aat*II−*Kpn*I restriction fragment of pR2-Y122F was ligated with the large (vector) fragment from digestion of pR2-W48F with the same

[2] Unpublished data from our laboratories.

restriction enzymes to yield pR2-W48F/Y122F. The 251 base pair *Bgl*II−*Aat*II restriction fragment (containing codons 1−52) from pR2-W48A was ligated with the large fragment from digestion of pR2-W48F/Y122F with the same endonucleases to give pR2-W48A/Y122F. The sequence of the coding region of each plasmid construct was verified to ensure that no undesired mutations had been introduced. DNA sequences were determined by the Nucleic Acid Facility of the Pennsylvania State University Biotechnology Institute.

The procedures used to isolate and quantify R2-W48A/Y122F were as described in the previous article (*43*). The value used for the molar absorption coefficient at 280 nm (ϵ_{280}) for R2-W48A/Y122F was 107 mM^{-1} cm^{-1}, as calculated by the procedure of Gill and von Hippel (*44*).

Preparation and Quantitation of Apo R2−W48A/D84E. Preparation of the expression vector for this protein is described elsewhere (*41*). The protein was purified as described in the preceding manuscript. It was quantified spectrophotometrically by assuming $\epsilon_{280} = 109$ mM^{-1} cm^{-1} (*44*).

Stopped-Flow Absorption Spectrophotometry. Stopped-flow absorption experiments were carried out with an Applied Photophysics SX.18MV stopped-flow apparatus equipped with a diode array detector and configured for sequential mixing (path length of 1 cm and dead time of 1.3 ms) or a Kintek Corporation model SF-2001 stopped-flow spectrofluorimeter equipped with a Gilford model 240 light source and configured for sequential mixing (path length 0.5 cm, dead time 3 ms). Both instruments were housed in an anoxic chamber (MBraun). Constant temperature was ensured with a Lauda K-4/R circulating water bath. Oxygen-free solutions of apo R2-W48A/Y122F in 100 mM Hepes buffer, 10% (v/v) glycerol, pH 7.6 (buffer A), oxygen-saturated solutions of buffer A, and oxygen-free stock solutions of 3-MI in ethanol (typically 100-fold more concentrated than the final concentration in the reaction) were prepared as described in the preceding paper (*43*). Stopped-flow measurements were carried out as previously described (*28*, *45*). Specific reaction conditions are given in the appropriate figure legends.

Freeze-Quench Electron Paramagnetic Resonance (EPR) and Mössbauer Experiments. The apparatus and procedures used to prepare the rapid freeze-quench EPR (RFQ-EPR) and Mössbauer (RFQ-Möss) samples have been described (*42*, *46*). Reaction conditions are given in the appropriate figure legends. The EPR and Mössbauer spectrometers have also been described (*28*, *46*). The spectrometer conditions are given in the figure legends.

Kinetic Simulations. The program KinTekSim (KinTek Corp., State College, PA) was used for simulation of kinetic data.

RESULTS

Preliminary Characterization of R2−W48A/Y122F. Preliminary characterization of the protein included determination of (1) the quantity of Fe(II) that it can take up and (2) whether the presence of ET mediator (3-MI) affects the products of its reaction with O_2. Addition of Fe(II) to the apo protein in the presence of O_2 leads to formation of absorbing products (Figure 1, dotted trace). Features of the

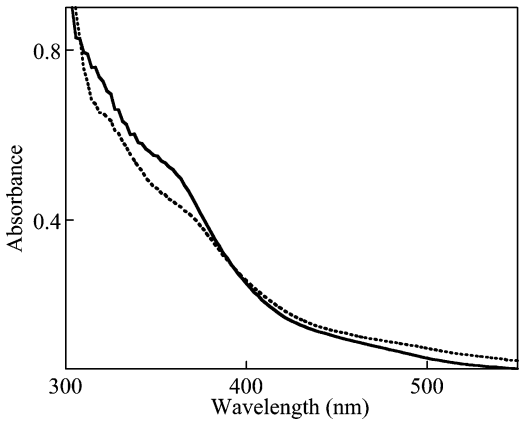

FIGURE 1: Light absorption spectra of the products of the reaction of Fe(II)−R2-W48A/Y122F (3.0 equiv of Fe) with excess O_2 in the absence (dotted trace) and presence (solid trace) of 1 mM 3-MI. The final protein concentration was 0.095 mM.

(μ-oxo)diiron(III) cluster at ~325 and ~365 nm (*4*) can be discerned, but the shape of the spectrum indicates that the normal cluster is not the sole product. The features are more prominent following addition of Fe(II) to the apo protein in the presence of 3-MI (solid trace), suggesting that ET mediation is effective in this variant. Titration of the apo protein with Fe(II) in the presence of 3-MI showed that 2.0−2.7 equiv is required for completion in our best preparations (used in this work). This stoichiometry is somewhat less than that for R2-wt (*20*) and several other variants (3.2 ± 0.2 equiv). In addition, the variation in this quantity from one preparation to another was greater than that for R2-wt or other variants. As was found for other variants with the W48A substitution (*43*), expression of the protein in 10% (v/v) glycerol was found to be required for achieving maximum Fe(II)-uptake capacity. Subsequent purification and maintenance of the protein in 10% glycerol rendered it completely stable with respect to Fe(II)-uptake capacity.

To verify the capacity of R2-W48A/Y122F to undergo ET mediation, the iron products formed upon addition of O_2 to the Fe(II)−R2-W48A/Y122F complex in the presence (+3-MI) and absence (−3-MI) of mediator were characterized by Mössbauer spectroscopy (Figure 2). As suggested by the optical absorption data, significantly (44%) more (μ-oxo)diiron(III) cluster is formed in the presence of the mediator (0.84 ± 0.08 equiv, spectrum B) than in its absence (0.58 ± 0.06 equiv, spectrum A). The increase in yield of the normal product in the presence of the mediator is much less pronounced than is observed for the R2-W48A reaction (see Figure 4 of the preceding manuscript (*43*)). The primary reason is *not* that ET mediation is less efficient in the double variant. Indeed, a product sample from the freeze-quench Mössbauer (RFQ-Möss) studies described below was found to contain 82% ± 3% (μ-oxo)diiron(III) cluster (Figure 2, spectrum C), nearly equivalent to the 88% ± 3% observed in a sample of R2-W48A prepared similarly (*43*). Instead, the less drastic increase in yield of the normal product is a reflection of the fact that more is formed in the −3-MI reaction of R2-W48A/Y122F than in the −3-MI reaction of the single variant. A similar observation was made previously in comparison of the products of the R2-W48F and R2-W48F/Y122F reactions. The normal (μ-oxo)diiron(III) cluster represents only ~25% of the products of the former (*42*) but nearly 60% of the products of the latter.[2] It seems that

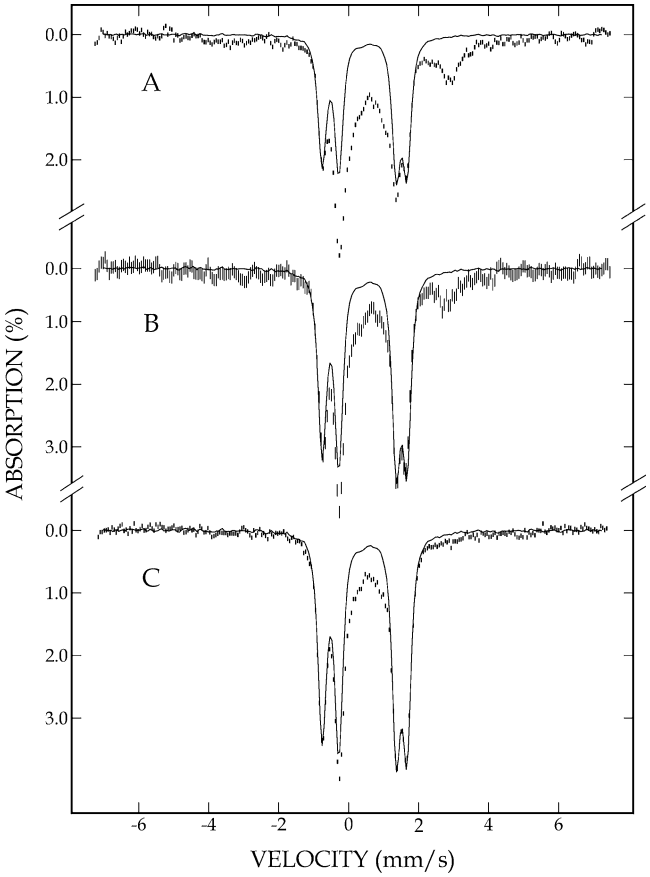

FIGURE 2: Mössbauer spectra of the products of the reaction of Fe(II)−R2-W48A/Y122F with excess O_2 (A) in the absence of 3-MI and (B) and (C) in the presence of 3-MI. For spectra A and B, the Fe(II)−R2-W48A/Y122F complex (2.3 equiv) was mixed at 5 ± 3 °C with an equal volume of O_2-saturated buffer, the reaction was allowed to proceed for 5 min, and the sample was frozen in a Mössbauer cup. The final protein concentration was 0.50 mM. Spectrum C is of a recovered product sample from the sequential-mixing experiment described in the legend to Figure 5, in which the Fe(II)−R2-W48A/Y122F complex (2.2 equiv of Fe) was mixed with O_2-saturated buffer, allowed to react at 11 °C for 0.20 s, mixed with an O_2-free solution of 3-MI (1 mM final concentration after mixing), and then allowed to age for 5 min prior to being frozen in a Mössbauer cell. The spectra were acquired at 4.2 K with a magnetic field of 50 mT applied parallel to the γ-beam. The solid lines plotted over the data in spectra A, B, and C are the experimental spectrum of the (μ-oxo)diiron(III) product from the reaction of Fe(II)−R2-wt with O_2 plotted at intensities corresponding to 51%, 73%, and 82%, respectively, of the experimental spectra.

the reaction pathway that precedes through the **X**−Y122$^{\bullet}$ diradical species, which is operant in R2-W48F(A) (*42*) but cannot be in R2-W48F(A)/Y122F, allows for more efficient formation of the altered Fe(III) products. In the absence of the oxidizable Y122, the normal product can form in higher yield even with the normal pathway for ET to the diiron cluster (*28*) disabled by substitution of W48 (*35, 42*). Nevertheless, the demonstration in Figure 2 that more of the normal product is produced in the +3-MI reaction confirms that the R2-W48A/Y122F reaction is indeed susceptible to ET mediation.

***S**topped-Flow Absorption and RFQ-Möss Evidence for Accumulation of an Intermediate*. In the reaction of the preformed Fe(II)−R2-W48A/Y122F complex with O_2 at 11 °C in the absence of 3-MI, three resolved kinetic phases can be discerned in the $A_{360\ nm}$-versus-time trace (Figure 3).

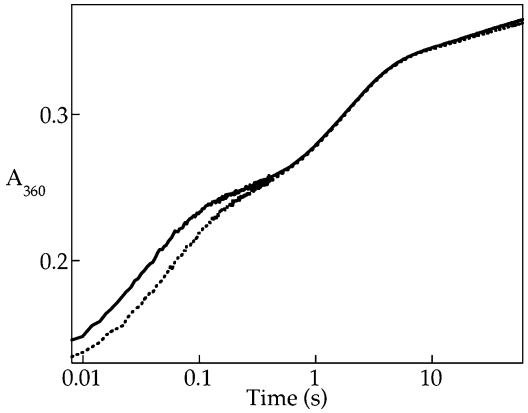

FIGURE 3: Kinetics of O_2 activation at 11 °C by Fe(II)−R2-W48A/Y122F monitored at 360 nm by stopped-flow absorption spectroscopy. Fe(II)−R2-W48A/Y122F (0.32 mM initial concentration, 3.0 equiv of Fe) was mixed in a volume ratio of 1:2 with either 100% O_2-saturated buffer (solid trace) or 50% O_2-saturated buffer (dotted trace). The final concentrations of O_2 were 0.6 mM (dotted trace) and 1.2 mM (solid trace).

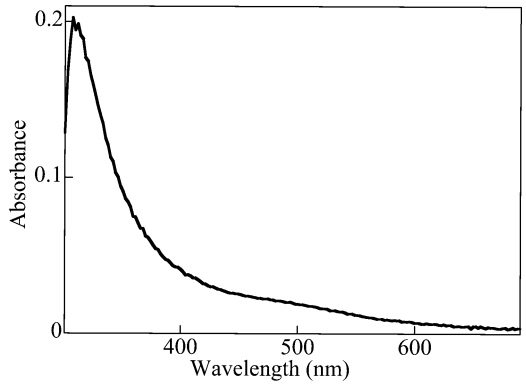

FIGURE 4: UV-visible absorption spectrum of intermediate species formed in the reaction of Fe(II)−R2-W48A/Y122F with O_2. Fe(II)−R2-W48A/Y122F (0.15 mM protein, 3.0 equiv of Fe) was mixed at 11 °C with an equal volume of O_2-saturated buffer. The spectrum is the change observed (i.e., a difference spectrum) during accumulation of the intermediate between t = 1.9 and 130 ms.

Fitting the equation for three parallel first-order processes to these data gave rate constants of 0.6 and 0.1 s^{-1} for the two slower phases. The rate of the fastest phase is dependent on the O_2 concentration (Figure 3, compare solid and dotted traces), implying that it is in this fast phase that O_2 adds to the diiron(II) cluster. Under the assumption that the slower phases represent subsequent steps in a sequence, the fact that the O_2-dependent phase is much faster implies that one or more intermediate species should accumulate to high levels. The absorption spectrum of this inferred adduct, which is obtained by subtraction of an early spectrum (~1.9 ms) from that corresponding to maximal accumulation of the intermediate (~130 ms), shows an absorption maximum at 310 nm and a shoulder at ~500 nm (Figure 4). Notably, absorption is not intense in the long-wavelength regime (600−725 nm) in which inorganic diiron(III) complexes that are known to have and protein complexes that are believed to have μ-1,2-peroxide bridges *do* absorb intensely (ϵ > 1000 M^{-1} s^{-1}) (*3, 13, 14, 16, 30*−*32, 41, 47*−*56*).

Mössbauer spectra at 4.2 K in a weak magnetic field (50 mT parallel to the γ-beam) of samples freeze-quenched during the fast, [O_2]-dependent phase of the reaction confirm the accumulation of an intermediate state. Features that are

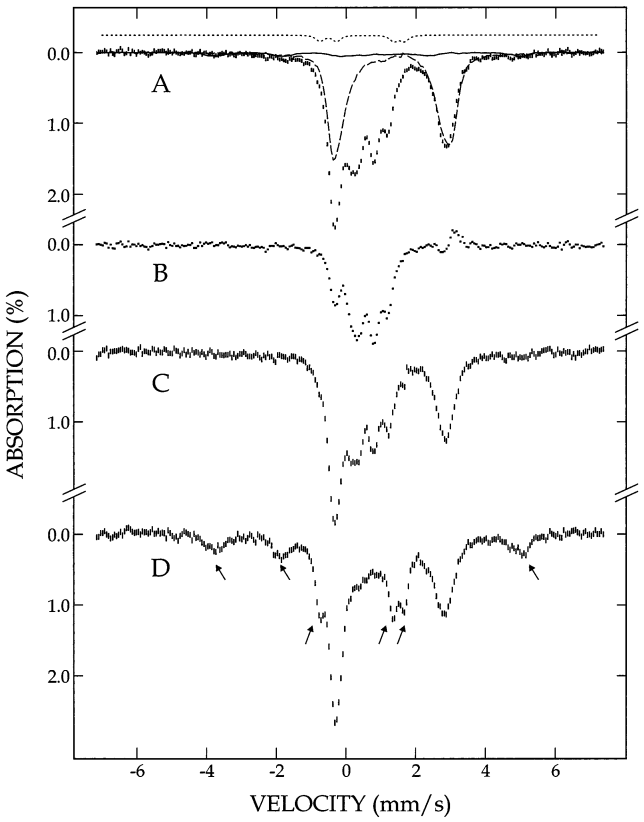

FIGURE 5: Mössbauer spectra from the reaction of Fe(II)−R2-W48A/Y122F with O_2 and the reaction of the resulting $(Fe_2O_2)^{4+}$ intermediate with 3-MI: (A) spectrum of a sample prepared by mixing Fe(II)−R2-W48A/Y122F (1.8 mM, 2.2 equiv of Fe) at 11 °C with an equal volume of O_2-saturated buffer and freeze-quenching 0.20 s after mixing; (B) spectrum of the intermediate obtained by removing the spectral contributions from contaminating species (50% Fe(II) reactant, dashed line plotted over data; 5% cluster **X**, solid line plotted over data; 3% (μ-oxo)diiron(III) product, dotted line plotted above data) from spectrum A. The reference spectrum for the Fe(II) reactant was of unreacted Fe(II)−R2-W48A/Y122F complex, and the reference spectra of **X** and the (μ-oxo)-diiron(III) product were derived from experimental spectra of samples from the reaction of Fe(II)−R2-wt with O_2. Spectra C and D are spectra of sequential-mix samples prepared by reaction of Fe(II)−R2-W48A/Y122F with O_2 (as in spectrum A), aging for 0.20 s, mixing of the resulting solution in a 2:1 volume ratio with either (C) O_2-free buffer or (D) O_2-free 3 mM 3-MI, and freeze-quenching 0.18 s after mixing. The spectra were acquired at 4.2 K with a magnetic field of 50 mT applied parallel to the γ-beam. The leftward and rightward slanting arrows below spectrum D point to the features of cluster **X** and the (μ-oxo)diiron(III) product, respectively.

not attributable to the reactant diiron(II) protein, cluster **X**, or the Fe(III) products develop rapidly (Figure 5, spectrum A) with kinetics consistent with those of the fast phase observed by stopped-flow. Following subtraction of the spectral contributions from the known species (solid, dashed, and dotted reference spectra plotted over and above the data in spectrum A), it can be seen that the rapidly developing new features are dominated by peaks at 0.3 and 0.8 mm/s with less intense peaks at approximately −0.3 and 1.2 mm/s (spectrum B). More definitive derivation of the spectrum of the intermediate state and analysis to extract Mössbauer parameters are presented below.

*Evidence for Conversion of the Intermediate to Cluster **X** Mediated by 3-MI.* The preceding paper demonstrates that ET can be mediated in W48A-containing variants by indole

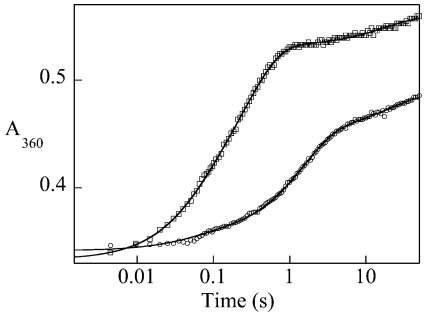

FIGURE 6: Reactivity of the putative $(Fe_2O_2)^{4+}$ intermediate species toward 3-MI as shown by stopped-flow absorption spectroscopy. Fe(II)−R2-W48A/Y122F (0.38 mM, 3.0 equiv of Fe) in buffer A was mixed at 11 °C with an equal volume of O_2-saturated buffer A. The solution was aged for 0.12 s before being mixed with an equal volume of either O_2-free 2 mM 3-MI solution (□) or O_2-free buffer A (○). The solid fit lines are the best fits of the equation describing three parallel first-order processes to the data.

compounds such as 3-MI (*43*). The above product analysis indicates that ET mediation is also effective in R2-W48A/Y122F. We next sought to test whether the intermediate state suggested by the stopped-flow and RFQ-Möss results would be induced to convert to cluster **X** by exposure to 3-MI. Fe(II)−R2-W48A/Y122F was mixed with O_2, the solution was aged for sufficient time for the intermediate state to accumulate to near-maximum levels (0.12 s), and the reaction solution was then mixed with an O_2-free solution of 3-MI (final concentration of 1 mM) or with O_2-free buffer (−3-MI control). In the −3-MI control (Figure 6, circles), the increase in absorbance at 360 nm corresponds to the two slower kinetic phases observed in Figure 3, with the majority of intensity associated with the faster of the two phases (apparent first-order rate constant of 0.6 s^{-1}). In the +3-MI experiment (Figure 6, squares), the increase in absorbance is much faster, and the amplitude is greater. An apparent first-order rate constant of 3.6 s^{-1} is obtained by regression analysis, suggesting that 3-MI accelerates the reaction by more than a factor of 5. Analysis of RFQ-EPR and RFQ-Möss data imply, however, that the reaction is accelerated to an even greater extent (see below).

RFQ-EPR was used to verify the capacity of 3-MI to accelerate decay of the putative intermediate. A sequential-mixing protocol essentially identical with that in the stopped-flow experiments was employed. The X-band EPR spectrum at 20 K of the experimental sample (Figure 7, solid spectrum), which was quenched 0.11 s after the preformed intermediate was mixed with 3-MI, exhibits the sharp, isotropic, $g = 2$ singlet characteristic of cluster **X** (*19, 20, 23, 29*). A much weaker signal (<20% of the integrated intensity) was observed for the −3-MI control sample quenched 0.11 s after a second mix with buffer (Figure 7, dashed spectrum). Kinetics of formation and decay of **X** after the mix with mediator (solid circles in Figure 8) or O_2-free buffer (triangles in Figure 8) were obtained (as previously described (*20*)) by double integration of the derivative EPR spectra of samples with varying second aging time.

The 3-MI-mediated conversion of the intermediate state to cluster **X** was further verified by RFQ-Möss. As before, the intermediate was allowed to accumulate after the first mix of Fe(II)−R2-W48A/Y122F with O_2 (aging time = 0.20 s), and the reaction solution was then mixed with O_2-free 3-MI (experiment) or O_2-free buffer (−3-MI control),

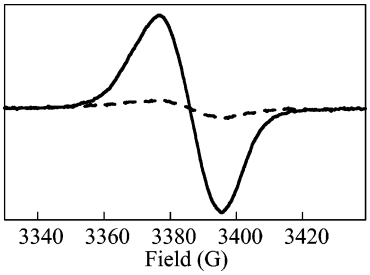

FIGURE 7: Reactivity of the putative $(Fe_2O_2)^{4+}$ intermediate species toward 3-MI as shown by sequential-mixing RFQ-EPR. Fe(II)−R2-W48A/Y122F (1.1 mM, 2.5 equiv of Fe) in buffer A was mixed at 11 °C with an equal volume of O_2-saturated buffer A. The solution was aged for 0.12 s before being mixed with an equal volume of either O_2-free 2 mM 3-MI solution (solid line) or O_2-free buffer A (dashed line). This solution was then aged for 0.11 s before being freeze-quenched. The spectra were acquired at 20 K. The spectrometer conditions were as follows: microwave frequency, 9.47 GHz; microwave power, 6.3 μW, modulation frequency, 100 kHz; modulation amplitude, 4.0 G; scan time, 330 s; time constant, 81 ms.

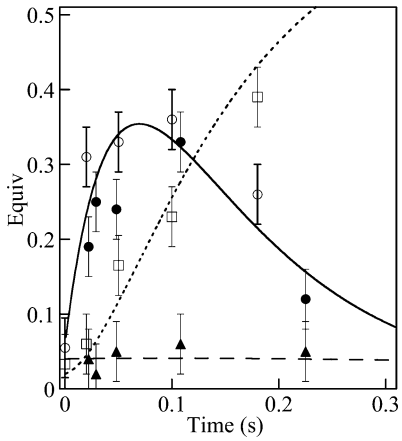

FIGURE 8: Quantities of **X** and the (μ-oxo)diiron(III) cluster as functions of time in reaction of the putative $(Fe_2O_2)^{4+}$ intermediate species with 3-MI (○ and □) or buffer (▲). The data are from analysis of Mössbauer (open symbols) and EPR (closed symbols) spectra of samples prepared as in the legends to Figures 5 and 7 (with varying second aging times). The circles and triangles depict the quantities of **X** and the squares the quantities of (μ-oxo)diiron-(III) cluster. The solid and dotted lines are simulations of the quantities of **X** and (μ-oxo)diiron(III) cluster, respectively, according to Scheme 1, an initial quantity of the $(Fe_2O_2)^{4+}$ intermediate of 0.6 equiv and rate constants given in the text. The dashed line plotted over the triangles is a simulation corresponding to 0.6 equiv of $(Fe_2O_2)^{4+}$ and rate constants of 0.6 and 8 s^{-1} for formation and decay of **X**. Both simulations take into account the small quantities of **X** and (μ-oxo)diiron(III) cluster formed in the first aging time, as indicated by the Mössbauer and EPR spectra of single-mix samples.

allowed to react for a second aging time, and then freeze-quenched. The weak-field/4.2 K Mössbauer spectra of control and experimental samples for which the second aging time was 0.18 s are shown in Figure 5 (spectra C and D, respectively). Comparison of the spectrum of the sample that was freeze-quenched after the initial accumulation phase of 0.20 s (A) to that of the sequential-mix −3-MI control (C) reveals that the reaction progresses to a minor extent (∼7−10% decay in the intensity of the features attributable to the intermediate) in 0.18 s in the absence of 3-MI. This result allows a rate constant of 0.4−0.6 s^{-1} to be estimated for the decay of the intermediate state in the absence of mediator. The spectrum of the experimental sample (D) exhibits the

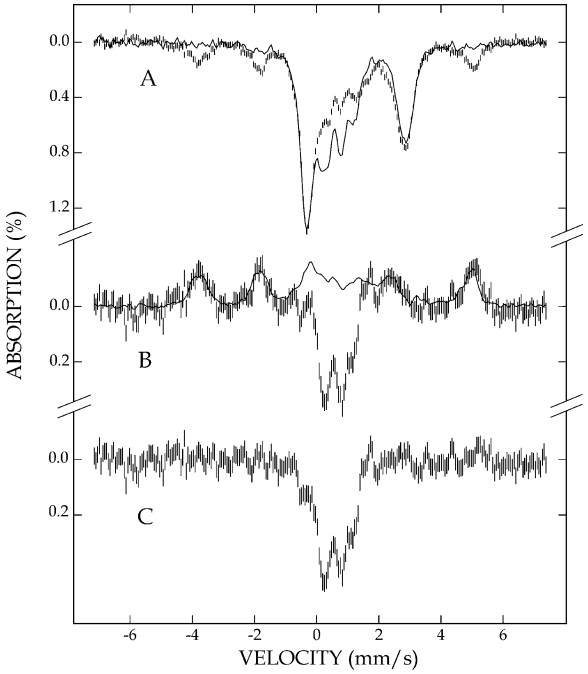

FIGURE 9: Kinetic resolution of the Mössbauer spectrum of the $(Fe_2O_2)^{4+}$ intermediate. The two overlaid spectra in A are of −3-MI control (solid line) and +3-MI experimental (hatches) samples prepared by the same procedure used to prepare those of Figure 5, spectra C and D, but with second aging times of 0.020 s. Spectrum B is the difference spectrum obtained by subtracting the spectrum of the experimental sample from that of the control sample. The solid line plotted over spectrum B is the summed (upward pointing) contributions from **X** and the (μ-oxo)diiron(III) cluster (23% and 4%, respectively). Spectrum C is the result of removing these contributions from spectrum B and represents the contributions of the $(Fe_2O_2)^{4+}$ state that decays upon mixing with 3-MI. The spectra were acquired at 4.2 K with a magnetic field of 50 mT applied parallel to the γ-beam.

paramagnetic signature of cluster **X** (leftward slanting arrows (*19*, *23*, *46*)) and the pair of quadrupole doublets characteristic of the (μ-oxo)diiron(III) product (rightward slanting arrows (*4*, *20*)). As importantly, the features of the intermediate state are absent, indicating that it decays in formation of **X** and the (μ-oxo)diiron(III) product. From analysis of spectra of samples with second aging times of 0.020 (see Figure 9), 0.050, 0.10, and 0.18 s, the kinetics of the 3-MI-mediated conversion of the intermediate state to cluster **X** (open circles in Figure 8) and the subsequent conversion of **X** to the (μ-oxo)diiron(III) product (open squares in Figure 8) were defined. The data (open symbols) are plotted in Figure 8 along with the quantities of **X** obtained by RFQ-EPR (solid symbols). All the kinetic data can be accounted for by assumption of rate constants of 22 s^{-1} for conversion of the $(Fe_2O_2)^{4+}$ intermediate state to cluster **X** and 8 s^{-1} for conversion of **X** to the (μ-oxo)diiron(III) product (Scheme 1) and an initial concentration of 0.6 equiv of $(Fe_2O_2)^{4+}$ relative to R2 dimer (solid and dotted traces in Figure 8). The magnitude of the rate constant for decay of **X** to the (μ-oxo)diiron(III) product, 8 s^{-1}, is perhaps larger than would have been expected. Decay of **X** in R2-Y122F has a rate constant of ∼0.3 s^{-1} at this temperature.[2] The comparison suggests that 3-MI accelerates *decay* of **X** in addition to its formation from its precursor. If this likelihood is neglected and it is assumed that decay of **X** in the absence of 3-MI also has a rate constant of 8 s^{-1}, then the kinetics of its

formation and decay in the absence of mediator can be accounted for reasonably well with a formation rate constant of 0.6 s^{-1} (Figure 8, dashed trace), consistent with the rate-constant estimated from the stopped-flow and RFQ-Möss data. Assumption of a smaller rate constant for decay of **X** in the absence of 3-MI would require an even smaller rate constant for its formation from the $(Fe_2O_2)^{4+}$ species to account for the failure of **X** to accumulate to a greater extent. Thus, 3-MI accelerates decay of the intermediate by at least 37-fold (22 s^{-1}/0.6 s^{-1}).

As indicated in Scheme 1, the 3-MI-mediated reduction of the $(Fe_2O_2)^{4+}$ complex to **X** should also produce a 3-MI radical. In principle, this might be detectable either by absorption at 310 and 510 nm (for a neutral radical) or at 335 and 560 nm (for a cation radical) (*57*) or by a $g \approx 2$ EPR signal. Attempts to detect spectral signatures of a transient 3-MI radical were unsuccessful. This observation suggests that, if a 3-MI radical forms in reduction of the $(Fe_2O_2)^{4+}$ complex to **X**, its decay is sufficiently rapid to prevent it from accumulating to a detectable level.

Nature of the Precursor to X as Revealed by RFQ-Möss. The single- and sequential-mixing SF-Abs, RFQ-EPR, and RFQ-Möss data establish that an intermediate state accumulates upon reaction of Fe(II)−R2-W48A/Y122F with O_2 and that this state is induced to convert rapidly to cluster **X** by the ET mediator, 3-MI. These results set the stage for the primary objective of this work, to obtain insight into the nature of the precursor to cluster **X** by resolution of its Mössbauer spectrum. The spectrum of this state was deduced by two independent "kinetic-difference" treatments. In the first, contributions of known "contaminants" (primarily diiron(II) reactant) to spectra of single-mix samples containing the intermediate were removed by subtraction of reference spectra for these species. This treatment amounts to a kinetic resolution of the features of the species that form (the intermediate state) in the first mix of Fe(II)−R2-W48A/Y122F with O_2 (the formation phase). An example was shown previously (Figure 5, spectrum B). In the second, subtraction of the spectrum of an experimental (+3-MI) sequential-mix RFQ-Möss sample (Figure 9, spectrum A, hatches) from the spectrum of the corresponding −3-MI control sample (spectrum A, solid line) generated a kinetic-difference spectrum (B) of the 3-MI-mediated reaction (the decay phase) with downward features from species that decay (the intermediate state) and upward features from species that form (**X** and the (μ-oxo)diiron(III) cluster). Removal of the upward contributions to this difference spectrum (solid line plotted over the data in spectrum B) then resolved the features of the species that decay (spectrum C). Two spectra from the formation phase (one derived from a sample with an aging time of 0.020 s, which is early in this phase, and one derived from a sample with an aging time of 0.20 s, which is essentially after completion of formation) and two from the decay phase (second aging times of 0.020 and 0.050 s) are shown in Figure 10. The spectra are qualitatively very similar. Each exhibits a broad central doublet with peaks at ∼0.3 and ∼0.8 mm/s and a less intense but sharper outer doublet with peaks at approximately −0.3 and 1.2 mm/s. Differences among the spectra can be attributed to uncertainties in the analysis and random error in the experimental spectra (of the samples and the "contaminating" species that must be accounted for). For example, the low-energy line

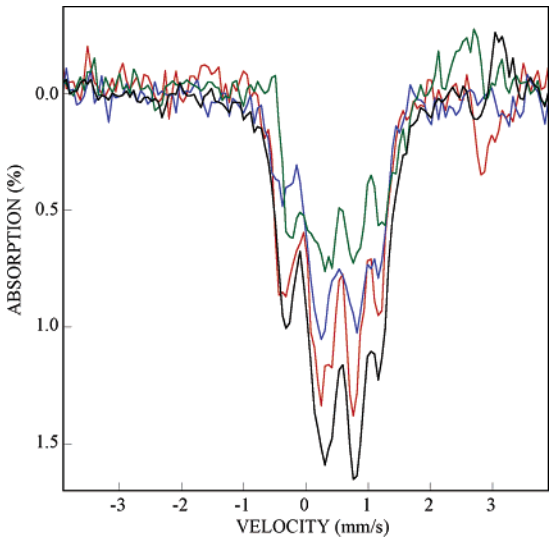

FIGURE 10: Four independent Mössbauer spectra of the $(Fe_2O_2)^{4+}$ intermediate. The spectra were derived by subtraction analysis of experimental spectra as described in the text and the legends to Figures 5 and 9. The green and black spectra are from the intermediate's formation phase (aging times of 0.020 and 0.20 s, respectively) and the blue and red spectra are from the decay phase (*second* aging times of 0.020 and 0.050 s, respectively).

of the weaker doublet is somewhat more variable in position, extent of resolution, and intensity than the three other peaks. This variation is attributable to imperfect removal of the contribution of Fe(II)-containing reactant, a problem that also leads to a small derivative-type artifact in the spectra at the position of the higher energy line of the Fe(II) complex (∼3 mm/s). Nevertheless, the four independent spectra obtained by two independent kinetic-resolution analyses agree quite well. This agreement is notable because the spectra from the formation phase were generated by removing contributions almost exclusively of Fe(II) reactant, whereas the spectra from the decay phase were generated by removing contributions exclusively from **X** and the (μ-oxo)diiron(III) product. The agreement proves that the intermediate state that converts to **X** by reaction with 3-MI is also the primary state that forms during the initial reaction with O_2. Moreover, the similarity of the kinetically resolved spectra constructed from samples quenched early or late in either the formation or the decay phase establishes that the complexes associated with the two sets of Mössbauer features form and decay together with complete kinetic correlation.

To decrease uncertainty in the spectrum of the intermediate state, the four independent, individual spectra from Figure 10 were averaged. In the averaging procedure, each spectrum was weighted according to the product of the relative contribution of the intermediate state to it and the baseline counts of the experimental spectrum used to generate it. The resulting spectrum was analyzed according to two alternative assumptions (Figure 11). Analysis of the spectrum by assumption of one inner and one outer quadrupole doublet yielded a relative intensity ratio of approximately 3:1 with Mössbauer parameters of $\delta = 0.52$ mm/s, and $\Delta E_Q = 0.55$ mm/s for the central doublet and $\delta = 0.45$ mm/s, $\Delta E_Q = 1.53$ mm/s for the outer doublet (solid line plotted over the data in Figure 11A). This analysis implies that the intermediate state comprises primarily two distinct diiron complexes, with each complex containing two Mössbauer-equivalent iron

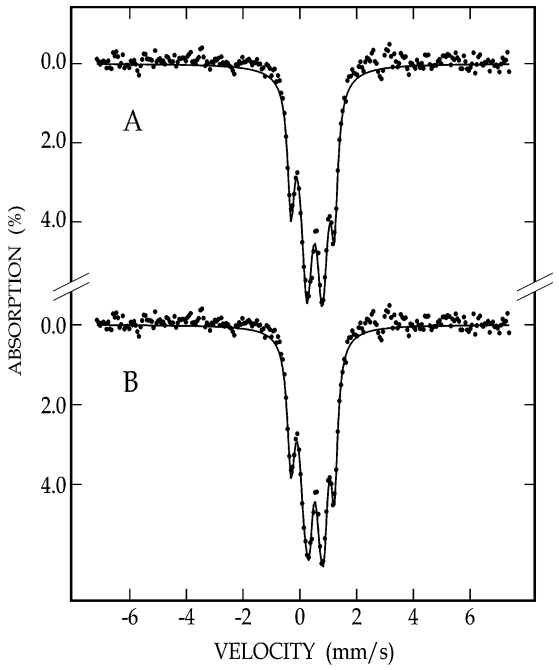

FIGURE 11: Analysis of the average derived spectrum of the $(Fe_2O_2)^{4+}$ intermediate. The spectrum was analyzed using two alternative assumptions. The solid line shown in spectrum A is a least-squares fit of the spectrum assuming one outer and one inner quadrupole doublet. The parameters obtained are $\Delta E_Q = 1.53$ mm/s, $\delta = 0.45$ mm/s, Γ (full width at half-maximum) $= 0.28$ mm/s, and percent absorption $= 23\%$ for the outer doublet and $\Delta E_Q = 0.55$ mm/s, $\delta = 0.52$ mm/s, $\Gamma = 0.48$ mm/s, and percent absorption $= 67\%$ for the inner doublet. The solid line shown in spectrum B is a least-squares fit of the spectrum assuming one outer and two inner quadrupole doublets. The outer doublet and one of the inner doublets are constrained to have the same percent absorption and line width to represent a diiron complex with inequivalent iron sites. The parameters obtained for the asymmetric complex are $\Delta E_Q(1) = 1.53$ mm/s, $\delta(1) = 0.45$ mm/s, $\Delta E_Q(2) = 0.53$ mm/s, $\delta(2) = 0.60$ mm/s, $\Gamma = 0.32$ mm/s, and a percent absorption of 27% for each doublet. The parameters for the unpaired inner doublet are $\Delta E_Q = 0.55$ mm/s, $\delta = 0.43$ mm/s, $\Gamma = 0.42$ mm/s, and a percent absorption of 36%.

sites. In consideration of the fact that the intermediate complexes are most likely peroxodiiron(III) species (vide infra) and that asymmetric oxygen binding has been observed for oxyhemerythrin (*58*), the peroxodiiron(III) intermediate in stearoyl acyl carrier protein Δ^9-desaturase (*52*), and several inorganic peroxodiiron(III) model complexes (*59, 60*), we also examined the possibility that the presence of asymmetric peroxide coordination leads to inequivalent Fe(III) sites in the intermediate state. The spectrum was thus least-squares fitted with one outer and two inner doublets. The outer doublet and one of the inner doublets were paired to represent an asymmetric complex and were therefore constrained to have the same intensity. Regardless of whether the line widths of each doublet were constrained to be equal or allowed to vary independently, the analysis yielded a rather constant δ of 0.6 mm/s and a narrow range of ΔE_Q, 0.43−0.53 mm/s for the inner doublet that was paired with the outer doublet. The parameters of the outer doublet and second (unpaired) inner doublet were changed to a minor extent from those obtained in the simpler two-doublet fit. The solid line plotted over the data in Figure 11B is a least-squares fit resulting from such an analysis. On the basis of the above spectral and kinetic analyses, the following conclusions can

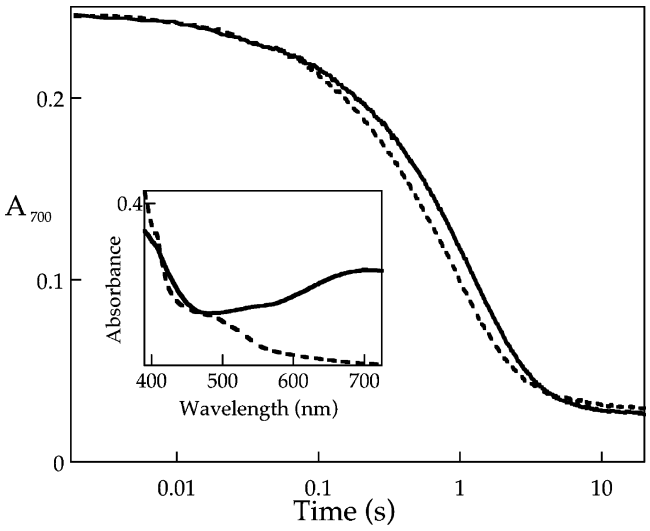

FIGURE 12: Inertness toward 3-MI-mediated reduction of the (μ-1,2-peroxo)diiron(III) complex that accumulates in the reaction of Fe(II)−R2-W48A/D84E with O_2. Fe(II)−R2-W48A/D84E (0.35 mM, 3.5 equiv of Fe) was mixed at 11 °C with an equal volume of O_2-saturated buffer. This solution was aged for 0.17 s prior to being mixed with an equal volume of either O_2-free buffer (solid line) or O_2-free 4 mM 3-MI solution (dotted line). The inset shows absorption spectra for the −3-MI control reaction shortly (3.2 ms) after the second mix (solid trace) and after completion (50 s, dotted trace) to illustrate the intense 700-nm absorption feature of the (μ-1,2-peroxo)diiron(III) complex that forms in the reactions of all R2 variants with the D84E substitution.

be made. The 3:1 intensity ratio of the central and outer doublets indicates that the intermediate state is heterogeneous: at least two Fe complexes are present. The invariance of the relative intensity of these doublets with time in both formation and decay phases of the reaction suggests that the two (or more) complexes exist in a rapid (with respect to formation and 3-MI-mediated decay) equilibrium. The Mössbauer parameters suggest that these complexes are composed of high-spin Fe(III) ions, and the lack of observed magnetic hyperfine interactions indicates that they are antiferromagnetically coupled diiron(III) clusters. Complexes either with nearly equivalent Fe(III) sites or with inequivalent, resolved Fe(III) sites are equally possible.

Reactivity of the (μ-1,2-Peroxo)diiron(III) Complex that Accumulates in D84E R2 Variants Toward 3-MI-Mediated Reduction. Peroxodiiron(III) complexes believed to have μ-1,2-peroxide bridges have been detected in reactions of O_2 with the reduced forms of a number of diiron-carboxylate proteins (MMOH (*13, 14, 16*), variants of R2 containing the D84E substitution (*30−32, 41*), chemically reduced stearoyl acyl carrier protein Δ^9-desaturase (*51, 52*), and ferritin (*53−55*)). These complexes are distinguished by their intense long-wavelength absorption (650−725 nm, $\epsilon > 1000$ M^{-1} cm^{-1}) and their unusually high (for high-spin Fe(III) species) Mössbauer isomer shifts (0.58−0.68 mm/s). As previously noted, observation of both optical and Mössbauer features potentially indicative of a similar complex in the reaction of Fe(II)−R2-wt with O_2 was reported in an earlier study (*22*). On this basis and the expectation that the structurally similar proteins would react with O_2 through common early intermediates (*1, 61*), a (μ-1,2-peroxo)diiron(III) complex has been proposed as an early intermediate in the R2 reaction (*1, 22, 38, 39, 48, 61−63*). Direct reduction of this complex by injection of the extra electron has also been invoked (*39,*

Scheme 2: Proposal That the $(Fe_2O_2)^{4+}$ Intermediate State Is a Successor to the (μ-1,2-Peroxo)diiron(III) Complex in the Reactions of (A) R2-wt, (B) R2-W48A/Y122F, and (C) R2-D84E and R2-W48F/D84E[a]

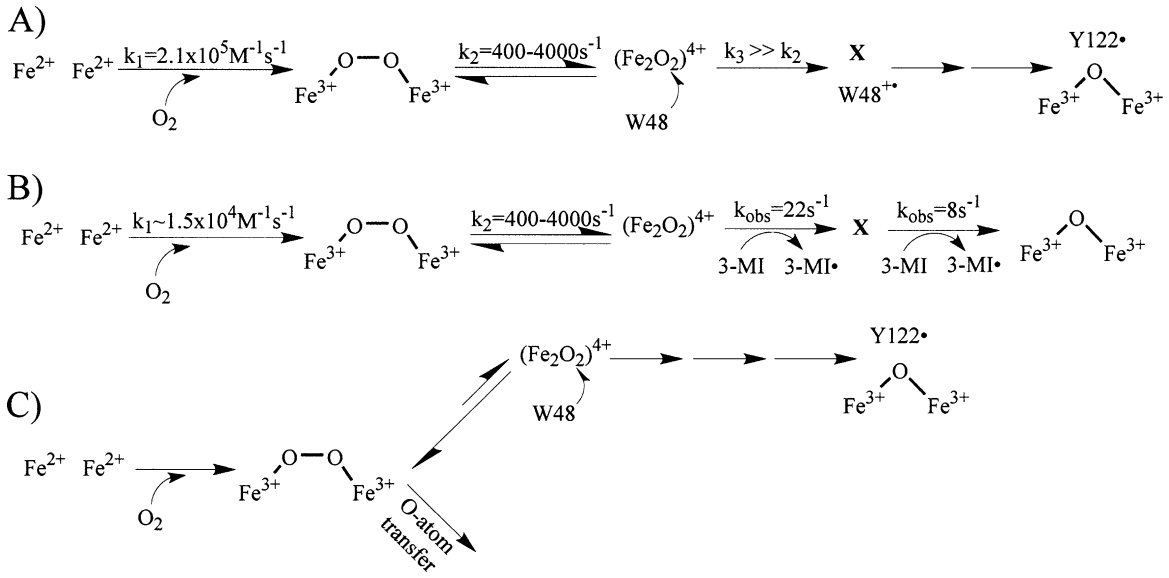

[a] Kinetic constants are from ref *28* (A) and this work (B).

62). To test the reactivity of a known (μ-1,2-peroxo)diiron(III) complex toward 3-MI-mediated reduction, sequential-mixing stopped-flow experiments were carried out with R2-W48A/D84E. As noted above, the D84E substitution causes the (μ-1,2-peroxo)diiron(III) complex to accumulate to stoichiometric levels (*30*−*32*, *41*). Evidence presented in the preceding paper establishes that this protein is also susceptible to ET mediation by 3-MI (*43*). Perhaps surprisingly, exposure of the (μ-1,2-peroxo)diiron(III) complex, formed in an initial incubation of Fe(II)−R2-W48A/D84E and O_2 (inset to Figure 12), to 1 mM 3-MI accelerates decay of the 700-nm absorption of the complex by less than 20% (main panel of Figure 12), despite the fact that the presence of the mediator results in formation of 2.2 times as much stable $Y122^{\bullet}$ (*43*). This result suggests that the (μ-1,2-peroxo)diiron(III) complex itself is unreactive toward 3-MI-mediated reduction and that 3-MI-mediated ET can occur only after the relatively inert complex decays to a more reactive species. Thus, both the spectroscopic properties of the (μ-1,2-peroxo)diiron(III) complex and its reactivity contrast markedly with those of the $(Fe_2O_2)^{4+}$ intermediate state in R2-W48A/Y122F.

DISCUSSION

The complexes that accumulate in the reaction of R2-W48A/Y122F and convert to cluster **X** upon exposure to 3-MI are clearly distinct from intermediates characterized to date in O_2 activation by diiron-carboxylate proteins. They have isomer shifts squarely in the range of high-spin Fe(III) species, ruling out the possibility that they are Fe(IV) complexes related to sMMO **Q** (*11*, *13*), and also lack the Mössbauer signature and intense low-energy optical absorption characteristic of (μ-1,2-peroxo)diiron(III) complexes such as **P** (*13*, *14*, *16*, *30*−*32*, *49*−*54*, *56*). Three possibilities must be considered concerning the relationship of the $(Fe_2O_2)^{4+}$ state to the normal (wt) R2 reaction sequence. First, the state may comprise off-pathway complexes that accumulate either (1) because the ET pathway is blocked and they are more stable than the complex that would otherwise rapidly oxidize W48 or (2) because the amino acid substitutions perturb the structure or dynamics of the protein, altering the reaction pathway. The issue of whether an intermediate detected in a variant protein is on the normal (wt) pathway is a general concern and was in this case the primary motivation for seeking a strategy to trigger the reactivity of the $(Fe_2O_2)^{4+}$ state that was previously inferred in the reactions of R2-W48F and R2-W48F/Y122F. With this strategy, the "chemical competence" of the $(Fe_2O_2)^{4+}$ state to convert to **X** has been unequivocally established. On this basis, we strongly disfavor the first possibility. Second, the state may comprise rapidly interconverting diiron(II)−O_2 complexes that form early in a pathway for O_2 activation that is orthogonal to that beginning with the (μ-1,2-peroxo)diiron(III) complex (as in sMMO and D84E R2 variants). This possibility would imply that the D84E substitution in R2 fundamentally changes the O_2 activation mechanism by causing an initial adduct with different geometry and reactivity to form. Under the assumption that the $(Fe_2O_2)^{4+}$ state formed with the wt ligands is reactive specifically toward one-electron reduction whereas the (μ-1,2-peroxo)diiron(III) complex is less reactive in this manner but more reactive toward O-atom transfer (either directly or after conversion to, for example, a diiron(IV) complex), this scenario would rationalize the observations that hydroxylation of the nearby F208 phenyl ring occurs in R2-W48F/D84E (even though Y122 is still present), whereas F208 hydroxylation does not occur in R2-W48F/Y122F (even though both residues that are facile donors of one electron to the $(Fe_2O_2)^{4+}$ state are absent) (*32*). However, this possibility would not accommodate the previous evidence for a **P**-like complex in the reaction of R2-wt (*22*), nor would it rationalize simply the observation that the **P**-like complex decays to form $Y122^{\bullet}$ in the reaction of R2-D84E (*30*). For these reasons, we favor the third possibility: that the detected intermediate state is a *successor* to the **P**-like complex (Scheme 2) in the R2-wt reaction pathway. This hypothesis can accommodate all the available data. With the measured rate constant for addition of O_2 in the R2-wt reaction (k_1 =

2.1×10^5 M^{-1} s^{-1} at 5 °C) (*28*), an appropriately large rate constant ($k_2 \approx 400-4000$ s^{-1}) for conversion of the initial **P**-like adduct to the $(Fe_2O_2)^{4+}$ intermediate state detected herein, and a still larger rate constant (k_3) for oxidation of W48 by the $(Fe_2O_2)^{4+}$ state, the accumulation of low levels of the **P**-like complex but none of the successor $(Fe_2O_2)^{4+}$ state would be rationalized (Scheme 2A). In the reactions of W48 variants, the observed ~10-fold slowing of O_2 addition (presumably due to a secondary effect of the substitution on protein or cluster dynamics) (*42*) would cause the (μ-1,2-peroxo)diiron(III) complex to be kinetically masked, and the block in ET would allow the successor $(Fe_2O_2)^{4+}$ complex to accumulate (Scheme 2B). The effect of the D84E substitution would then be explained in terms of a retardation of the conversion of the **P**-like complex to the $(Fe_2O_2)^{4+}$ state, an effect on the equilibrium for this conversion, or both (Scheme 2C). Reversibility in this conversion could rationalize the fact that decay of the (μ-1,2-peroxo)diiron(III) complex in D84E variants can lead either to $Y122^{\bullet}$ formation (with the electron-shuttling W48 present) or to F208 hydroxylation (with W48 replaced by F). If isomerization of the **P**-like complex to the $(Fe_2O_2)^{4+}$ state is still faster than the competing step that commits the reaction to O-atom transfer (F208 hydroxylation), efficient one-electron reduction of the $(Fe_2O_2)^{4+}$ state by W48 (upper pathway in Scheme 2C) would make the one-electron-oxidation outcome predominant. In the absence of efficient reduction, the $(Fe_2O_2)^{4+}$ state would partition back to the (μ-1,2-peroxo)diiron(III) complex, which would persist long enough to enter the O-atom transfer pathway (lower pathway in Scheme 2C). The very modest effect of 3-MI on the kinetics of decay of the (μ-1,2-peroxo)diiron(III) complex in the R2-W48A/D84E reaction would be explained by the fact that prior isomerization to the $(Fe_2O_2)^{4+}$ state is required and is relatively slow. Thus, our working hypothesis is that the $(Fe_2O_2)^{4+}$ state is part of the R2-wt reaction pathway and is a successor to the expected (μ-1,2-peroxo)diiron(III) complex. This hypothesis would imply that the point of divergence of the R2 and sMMO mechanisms is in the fate of the common (μ-1,2-peroxo)diiron(III) adduct: O−O bond cleavage to generate the methane-hydroxylating diiron(IV) complex, **Q**, in sMMO as opposed to isomerization to the one-electron-oxidizing $(Fe_2O_2)^{4+}$ state in R2. The presence of aspartate at position 84 in R2 (as opposed to glutamate at the corresponding position of MMOH) would be seen as an adaptation to favor the conversion of the initial intermediate to the complex that is more reactive for one-electron reduction.

At present, it is impossible to say what the structures of the complexes in the $(Fe_2O_2)^{4+}$ intermediate state might be. The deduced Mössbauer parameters do not match those of any structurally characterized complex of which we are aware. Complicating the situation further is the fact that it is impossible to choose between the two alternative analyses corresponding to (1) two diiron complexes with relative abundance ~1:3 (outer doublet/inner doublet) and unresolved Fe sites or (2) two complexes, one with inequivalent and resolved Fe sites (the outer doublet and paired inner doublet) and one with unresolved Fe sites (the second inner doublet), at relative abundances of 1.5:1. There is ample precedent for the site inequivalency required by the latter analysis (*52*, *58*−*60*), but the absence of either spectral or kinetic resolution of the presumed two doublets constituting the broad inner features precludes an unambiguous choice of the correct analysis. In principle, application of additional spectroscopic methods (e.g., resonance Raman or extended x-ray absorption fine structure (EXAFS)) could yield more detailed structural insight, but its lack of a strong visible chromophore and the heterogeneity of the state will mitigate against these approaches. Synthetic inorganic chemistry and density functional theory (DFT) calculations are perhaps more likely to yield greater structural insight. These studies should seek to identify a pair of peroxodiiron(III) complexes that are distinct from the **P**-like (presumably (μ-1,2-peroxo)-diiron(III)) structure and that have similar free energies and a low barrier for interconversion. Arguably, the complexes should be favored thermodynamically over the **P**-like complex for the case of addition of O_2 to the diiron(II) cluster with the wt ligand sphere but disfavored relative to the **P**-like complex in R2 variants with the D84E substitution. Correlation of experimental Mössbauer parameters with those determined for model complexes or calculated for the computationally derived structures might then be used to validate candidate structures. We are pursuing these and other strategies to clarify the nature of the $(Fe_2O_2)^{4+}$ state.

REFERENCES

1. Nordlund, P., and Eklund, H. (1995) Di-iron-carboxylate proteins, *Curr. Opin. Struct. Biol. 5*, 758−766.
2. Wallar, B. J., and Lipscomb, J. D. (1996) Dioxygen activation by enzymes containing binuclear non-heme iron clusters, *Chem. Rev. 96*, 2625−2657.
3. Solomon, E. I., Brunold, T. C., Davis, M. I., Kemsley, J. N., Lee, S.-K., Lehnert, N., Neese, F., Skulan, A. J., Yang, Y.-S., and Zhou, J. (2000) Geometric and electronic structure/function correlations in non-heme iron enzymes, *Chem. Rev. 100*, 235−349.
4. Atkin, C. L., Thelander, L., and Reichard, P. (1973) Iron and free radical in ribonucleotide reductase. Exchange of iron and Mössbauer spectroscopy of the protein B2 subunit of the *Escherichia coli* enzyme, *J. Biol. Chem. 248*, 7464−7472.
5. Sjöberg, B.-M., Reichard, P., Gräslund, A., and Ehrenberg, A. (1977) Nature of the free radical in ribonucleotide reductase from *Escherichia coli*, *J. Biol. Chem. 252*, 536−541.
6. Larsson, A., and Sjöberg, B.-M. (1986) Identification of the stable free radical tyrosine residue in ribonucleotide reductase, *EMBO J. 5*, 2037−2040.
7. Dalton, H. (1980) Oxidation of hydrocarbons by methane monooxygenases from a variety of microbes, *Adv. Appl. Microbiol. 26*, 71−87.
8. Woodland, M. P., Patil, D. S., Cammack, R., and Dalton, H. (1986) ESR studies of protein A of the soluble methane monooxygenase from *Methylococcus capsulatus* (Bath), *Biochim. Biophys. Acta 873*, 237−242.
9. Fox, B. G., Surerus, K. K., Münck, E., and Lipscomb, J. D. (1988) Evidence for a μ-oxo-bridged binuclear iron cluster in the hydroxylase component of methane monooxygenase. Mössbauer and EPR studies, *J. Biol. Chem. 263*, 10553−10556.
10. Merkx, M., Kopp, D. A., Sazinsky, M. H., Blazyk, J. L., Müller, J., and Lippard, S. J. (2001) Dioxygen activation and methane hydroxylation by soluble methane monooxygenase: a tale of two irons and three proteins, *Angew. Chem., Int. Ed. 40*, 2782−2807.
11. Lee, S.-K., Fox, B. G., Froland, W. A., Lipscomb, J. D., and Münck, E. (1993) A transient intermediate of the methane monooxygenase catalytic cycle containing an $Fe^{IV}Fe^{IV}$ cluster, *J. Am. Chem. Soc. 115*, 6450−6451.
12. Lee, S.-K., Nesheim, J. C., and Lipscomb, J. D. (1993) Transient intermediates of the methane monooxygenase catalytic cycle, *J. Biol. Chem. 268*, 21569−21577.
13. Liu, K. E., Wang, D., Huynh, B. H., Edmondson, D. E., Salifoglou, A., and Lippard, S. J. (1994) Spectroscopic detection of intermediates in the reaction of dioxygen with the reduced methane monooxygenase/hydroxylase from *Methylococcus capsulatus* (Bath), *J. Am. Chem. Soc. 116*, 7465−7466.

14. Liu, K. E., Valentine, A. M., Wang, D., Huynh, B. H., Edmondson, D. E., Salifoglou, A., and Lippard, S. J. (1995) From the mass production of *Methylococcus capsulatus* to the efficient separation and isolation of methane monooxygenase proteins. Characterization of novel intermediates in substrate reactions of methane monooxygenase, *J. Am. Chem. Soc. 117*, 10174−10185.
15. Shu, L. J., Nesheim, J. C., Kauffmann, K., Münck, E., Lipscomb, J. D., and Que, L., Jr. (1997) An $Fe_2^{IV}O_2$ diamond core structure for the key intermediate Q of methane monooxygenase, *Science 275*, 515−518.
16. Valentine, A. M., Stahl, S. S., and Lippard, S. J. (1999) Mechanistic studies of the reaction of reduced methane monooxygenase hydroxylase with dioxygen and substrates, *J. Am. Chem. Soc. 121*, 3876−3887.
17. Lee, S.-K., and Lipscomb, J. D. (1999) Oxygen activation catalyzed by methane monooxygenase hydroxylase component: proton delivery during the O−O bond cleavage steps, *Biochemistry 38*, 4423−4432.
18. Brazeau, B. J., and Lipscomb, J. D. (2000) Kinetics and activation thermodynamics of methane monooxygenase compound Q formation and reaction with substrates, *Biochemistry 39*, 13503−13515.
19. Bollinger, J. M., Jr., Stubbe, J., Huynh, B. H., and Edmondson, D. E. (1991) Novel diferric radical intermediate responsible for tyrosyl radical formation in assembly of the cofactor of ribonucleotide reductase, *J. Am. Chem. Soc. 113*, 6289−6291.
20. Bollinger, J. M., Jr., Tong, W. H., Ravi, N., Huynh, B. H., Edmondson, D. E., and Stubbe, J. (1994) Mechanism of assembly of the tyrosyl-diiron(III) cofactor of *E. coli* ribonucleotide reductase. 2. Kinetics of the excess Fe^{2+} reaction by optical, EPR, and Mössbauer spectroscopies, *J. Am. Chem. Soc. 116*, 8015−8023.
21. Bollinger, J. M., Jr., Tong, W. H., Ravi, N., Huynh, B. H., Edmondson, D. E., and Stubbe, J. (1994) Mechanism of assembly of the tyrosyl radical-diiron(III) cofactor of *E. coli* ribonucleotide reductase. 3. Kinetics of the limiting Fe^{2+} reaction by optical, EPR, and Mössbauer spectroscopies, *J. Am. Chem. Soc. 116*, 8024−8032.
22. Tong, W. H., Chen, S., Lloyd, S. G., Edmondson, D. E., Huynh, B. H., and Stubbe, J. (1996) Mechanism of assembly of the diferric cluster-tyrosyl radical cofactor of *Escherichia coli* ribonucleotide reductase from the diferrous form of the R2 subunit, *J. Am. Chem. Soc. 118*, 2107−2108.
23. Sturgeon, B. E., Burdi, D., Chen, S., Huynh, B. H., Edmondson, D. E., Stubbe, J., and Hoffman, B. M. (1996) Reconsideration of X, the diiron intermediate formed during cofactor assembly in *E. coli* ribonucleotide reductase, *J. Am. Chem. Soc. 118*, 7551−7557.
24. Burdi, D., Sturgeon, B. E., Tong, W. H., Stubbe, J., and Hoffman, B. M. (1996) Rapid freeze-quench ENDOR of the radical X intermediate of *Escherichia coli* ribonucleotide reductase using $^{17}O_2$ and $H_2{}^{17}O$. *J. Am. Chem. Soc. 118*, 281−282.
25. Willems, J.-P., Lee, H.-I., Burdi, D., Doan, P. E., Stubbe, J., and Hoffman, B. M. (1997) Identification of the protonated oxygenic ligands of ribonucleotide reductase intermediate X by Q-Band ^{1,2}H CW and pulsed ENDOR. *J. Am. Chem. Soc. 119*, 9816−9824.
26. Burdi, D., Willems, J.-P., Riggs-Gelasco, P., Antholine, W. E., Stubbe, J., and Hoffman, B. M. (1998) The core structure of X generated in the assembly of the diiron cluster of ribonucleotide reductase: $^{17}O_2$ and $H_2{}^{17}O$ ENDOR, *J. Am. Chem. Soc. 120*, 12910−12919.
27. Riggs-Gelasco, P. J., Shu, L., Chen, S., Burdi, D., Huynh, B. H., Que, L., Jr., and Stubbe, J. (1998) EXAFS characterization of the intermediate X generated during the assembly of the *Escherichia coli* ribonucleotide reductase R2 diferric tyrosyl radical cofactor, *J. Am. Chem. Soc. 120*, 849−860.
28. Baldwin, J., Krebs, C., Ley, B. A., Edmondson, D. E., Huynh, B. H., and Bollinger, J. M., Jr. (2000) Mechanism of rapid electron transfer during oxygen activation in the R2 subunit of *Escherichia coli* ribonucleotide reductase. 1. Evidence for a transient tryptophan radical, *J. Am. Chem. Soc. 122*, 12195−12206.
29. Bollinger, J. M., Jr., Edmondson, D. E., Huynh, B. H., Filley, J., Norton, J. R., and Stubbe, J. (1991) Mechanism of assembly of the tyrosyl radical-dinuclear iron cluster cofactor of ribonucleotide reductase, *Science 253*, 292−298.
30. Bollinger, J. M., Jr., Krebs, C., Vicol, A., Chen, S., Ley, B. A., Edmondson, D. E., and Huynh, B. H. (1998) Engineering the diiron site of *Escherichia coli* ribonucleotide reductase protein R2 to accumulate an intermediate similar to H_{peroxo}, the putative peroxodiiron(III) complex from the methane monooxygenase catalytic cycle, *J. Am. Chem. Soc. 120*, 1094−1095.
31. Moënne-Loccoz, P., Baldwin, J., Ley, B. A., Loehr, T. M., and Bollinger, J. M., Jr. (1998) O_2 activation by non-heme diiron proteins: Identification of a symmetric μ-1,2-peroxide in a mutant of ribonucleotide reductase, *Biochemistry 37*, 14659−14663.
32. Baldwin, J., Voegtli, W. C., Khidelkel, N., Moënne-Loccoz, P., Krebs, C., Pereira, A. S., Ley, B. A., Huynh, B. H., Loehr, T. M., Riggs-Gelasco, P. J., Rosenzweig, A. C., and Bollinger, J. M., Jr. (2001) Rational reprogramming of the R2 subunit of *Escherichia coli* ribonucleotide reductase into a self-hydroxylating monooxygenase, *J. Am. Chem. Soc. 123*, 7017−7030.
33. Ormö, M., deMaré, F., Regnström, K., Åberg, A., Sahlin, M., Ling, J., Loehr, T. M., Sanders-Loehr, J., and Sjöberg, B.-M. (1992) Engineering of the iron site in ribonucleotide reductase to a self-hydroxylating monoxygenase, *J. Biol. Chem. 267*, 8711−8714.
34. Åberg, A., Ormö, M., Nordlund, P., and Sjöberg, B.-M. (1993) Autocatalytic generation of dopa in the engineered protein R2 F208Y from *Escherichia coli* ribonucleotide reductase and crystal structure of the dopa 208 protein, *Biochemistry 32*, 9845−9850.
35. Parkin, S. E., Chen, S., Ley, B. A., Mangravite, L., Edmondson, D. E., Huynh, B. H., and Bollinger, J. M., Jr. (1998) Electron injection through a specific pathway determines the outcome of oxygen activation at the diiron cluster in the F208Y mutant of *Escherichia coli* ribonucleotide reductase protein R2, *Biochemistry 37*, 1124−1130.
36. Logan, D. T., deMaré, F., Persson, B. O., Slaby, A., Sjöberg, B.-M., and Nordlund, P. (1998) Crystal structures of two self-hydroxylating ribonucleotide reductase protein R2 mutants: structural basis for the oxygen-insertion step of hydroxylation reactions catalyzed by diiron proteins, *Biochemistry 57*, 10798−10807.
37. Valentine, A. M., Tavares, P., Pereira, A. S., Davydov, R., Krebs, C., Hoffman, B. M., Edmondson, D. E., Huynh, B. H., and Lippard, S. J. (1998) Characterization of a mixed-valent Fe(III)-Fe(IV) form of intermediate Q in the reaction cycle of soluble methane monooxygenase, an analogue of intermediate X in ribonucleotide reductase R2 assembly, *J. Am. Chem. Soc. 120*, 2190−2191.
38. Yang, Y.-S., Baldwin, J., Ley, B. A., Bollinger, J. M., Jr., and Solomon, E. I. (2000) Spectroscopic and electronic structure description of the reduced binuclear non-heme iron active site in ribonucleotide reductase from *E. coli*: Comparison to reduced Δ^9 desaturase and electronic structure contributions to differences in O_2 reactivity, *J. Am. Chem. Soc. 122*, 8495−8510.
39. Siegbahn, P. E. M. (2002) A comparison of dioxygen bond cleavage in RNR and methane monooxygenase, *Chem. Phys. Lett. 351*, 311−318.
40. Torrent, M., Djamaladdin, G. M., Basch, H., and Morokuma, K. (2002) Computational studies of reaction mechanisms of methane monooxygenase and ribonucleotide reductase, *J. Comput. Chem. 23*, 59−76.
41. Baldwin, J., Krebs, C., Saleh, L., Stelling, M., Huynh, B. H., Bollinger, J. M., Jr., and Riggs-Gelasco, P. (2003) Structural characterization of the peroxodiiron(III) intermediate generated during oxygen activation by the W48A/D84E variant of ribonucleotide reductase protein R2 from *Escherichia coli*, *Biochemistry 42*, 13269−13279.
42. Krebs, C., Chen, S., Baldwin, J., Ley, B. A., Patel, U., Edmondson, D. E., Huynh, B. H., and Bollinger, J. M., Jr. (2000) Mechanism of rapid electron transfer during oxygen activation in the R2 subunit of *Escherichia coli* ribonucleotide reductase. 2. Evidence for and consequences of blocked electron transfer in the W48F variant, *J. Am. Chem. Soc. 122*, 12207−12219.
43. Saleh, L., Kelch, B. A., Pathickal, B. A., Baldwin, J., Ley, B. A., and Bollinger, J. M., Jr. (2004) Mediation by indole analogues of electron transfer during oxygen activation in variants of *Escherichia coli* ribonucleotide reductase R2 lacking the electron-shuttling tryptophan 48, *Biochemistry 43*, 5943−5952.
44. Gill, S. C., and von Hippel, P. H. (1989) Calculation of protein extinction coefficients from amino acid sequence data, *Anal. Biochem. 182*, 319−326.
45. Yun, D., Krebs, C., Gupta, G. P., Iwig, D. F., Huynh, B. H., and Bollinger, J. M., Jr. (2002) Facile electron transfer during formation of cluster X and kinetic competence of X for tyrosyl radical production in protein R2 of ribonucleotide reductase from mouse, *Biochemistry 41*, 981−990.
46. Ravi, N., Bollinger, J. M., Jr., Huynh, B. H., Edmondson, D. E., and Stubbe, J. (1994) Mechanism of assembly of the tyrosyl radical-diiron(III) cofactor of *E. coli* ribonucleotide reductase: 1. Mössbauer characterization of the diferric radical precursor, *J. Am. Chem. Soc. 116*, 8007−8014.

47. Dong, Y., Yan, S., Young, V. G., Jr., and Que, L., Jr. (1996) Crystal structure analysis of a synthetic non-heme diiron-O_2 adduct: insight into the mechanism of oxygen activation, *Angew. Chem., Int. Ed. Engl 35*, 618−620.
48. Dong, Y., Zang, Y., Shu, L., Wilkinson, L., and Que, L., Jr. (1997) Models for non-heme diiron enzymes. Assembly of a high-valent $Fe_2(\mu\text{-}O)_2$ diamond core from its peroxo precursor, *J. Am. Chem. Soc. 119*, 12683−12684.
49. Kim, K., and Lippard, S. J. (1996) Structure and Mössbauer spectrum of a (μ-1,2-peroxo)bis(μ-carboxylato)diiron(III) model for the peroxo intermediate in the methane monooxygenase hydroxylase cycle, *J. Am. Chem. Soc. 118*, 4914−4915.
50. Ookubo, T., Sugimoto, H., Nagayama, T., Masuda, H., Sato, T., Tanaka, K., Maeda, Y., Okawa, H., Hayashi, Y., Uehara, A., and Suzuki, M. (1996) *cis*-μ-1,2-Peroxo Diiron Complex: Structure and Reversible Oxygenation, *J. Am. Chem. Soc. 118*, 701−702.
51. Broadwater, J. A., Ai, J., Loehr, T. M., Sanders-Loehr, J., and Fox, B. G. (1998) Peroxodiferric intermediate of stearoyl-acyl carrier protein Δ9 desaturase: oxidase reactivity during single turnover and implications for the mechanism of desaturation, *Biochemistry 37*, 14664−14671.
52. Broadwater, J. A., Achim, C., Münck, E., and Fox, B. G. (1999) Mössbauer studies of the formation and reactivity of a quasi-stable peroxo intermediate of stearoyl-acyl carrier protein ∂9-desaturase, *Biochemistry 38*, 12197−12204.
53. Pereira, A. S., Small, W., Krebs, C., Tavares, P., Edmondson, D. E., Theil, E. C., and Huynh, B. H. (1998) Direct spectroscopic and kinetic evidence for the involvement of a peroxodiferric intermediate during the ferroxidase reaction in fast ferritin mineralization, *Biochemistry 37*, 9871−9876.
54. Moënne-Loccoz, P., Krebs, C., Herlihy, K., Edmondson, D. E., Theil, E. C., Huynh, B. H., and Loehr, T. M. (1999) The ferroxidase reaction of ferritin reveals a diferric μ-1,2 bridging peroxide intermediate in common with other O_2-activating non-heme diiron proteins, *Biochemistry 38*, 5290−5295.
55. Huang, J., Krebs, C., Huynh, B. H., Edmondson, D. E., Theil, E. C., and Penner-Hahn, J. E. (2000) A short Fe−Fe distance in peroxodiferric ferritin: control of Fe substrate versus cofactor decay? *Science 287*, 122−125.
56. Brunold, T. C., Tamura, N., Kitajima, N., Moro-oka, Y., and Solomon, E. I. (1998) Spectroscopic study of $[Fe_2(O_2)(OBz)_2\{HB(pz')_3\}_2]$: Nature of the μ-1,2 peroxide-Fe(III) bond and its possible relevance to O_2 activation by non-heme iron enzymes, *J. Am. Chem. Soc. 120*, 5674−5690.
57. Solar, S., Getoff, N., Surdhar, P. S., Armstrong, D. A., and Sing, A. (1991) Oxidation of tryptophan and N-methylindole by $N_3^{\bullet}$, Br_2^-, and $(SCN)_2^-$ radicals in light- and heavy-water solutions: A pulse radiolysis study. *J. Phys. Chem. 95*, 3639−3643.
58. Que, L., Jr., and True, A. E. (1990) Dinuclear iron- and manganese-oxo sites in biology, in *Progress in Inorganic Chemistry* (Lippard, S. J., Ed.) pp 97−200, John Wiley & Sons, New York.
59. Mizoguchi, T. J., Kuzelka, J., Spingler, B., DuBois, J. L., Davydov, R. M., Hedman, B., Hodgson, K. O., and Lippard, S. J. (2001) Synthesis and spectroscopic studies of non-heme diiron(III) species with a terminal hydroperoxide ligand: Models for hemerythrin, *Inorg. Chem. 40*, 4662−4673.
60. He, C., Barrios, A. M., Lee, D., Kuzelka, J., Davydov, R. M., and Lippard, S. J. (2000) Diiron complexes of 1,8-naphthyridine-based dinucleating ligands as models for hemerythrin, *J. Am. Chem. Soc. 122*, 12683−12690.
61. Edmondson, D. E., and Huynh, B. H. (1996) Diiron-cluster intermediates in biological oxygen activation reactions, *Inorg. Chim. Acta 252*, 399−404.
62. Stubbe, J., and Riggs-Gelasco, P. (1998) Harnessing free radicals: formation and function of the tyrosyl radical in ribonucleotide reductase, *Trends Biochem. Sci. 23*, 438−443.
63. Andersson, M. E., Högbom, M., Rinaldo-Matthis, A., Andersson, K. K., Sjöberg, B.-M., and Nordlund, P. (1999) The crystal structure of an azide complex of the diferrous R2 subunit of ribonucleotide reductase displays a novel carboxylate shift with important mechanistic implications for diiron-catalyzed oxygen activation, *J. Am. Chem. Soc. 121*, 2346−2352.

BI036099E